Improved energy density and charge-discharge efficiency in solution processed highly defined ferroelectric block copolymer-based dielectric nanocomposites

Meereboer, Niels L.; Terzic, Ivan; Portale, Giuseppe; Loos, Katja

Published in:
Nano energy

DOI:
10.1016/j.nanoen.2019.103939

Publication date:
2019

Nano Energy 64 (2019) 103939

Contents lists available at ScienceDirect

Nano Energy

journal homepage: www.elsevier.com/locate/nanoen

Full paper

Improved energy density and charge-discharge efficiency in solution processed highly defined ferroelectric block copolymer-based dielectric nanocomposites

Niels L. Meereboer[1], Ivan Terzić[1], Giuseppe Portale, Katja Loos[*]

Macromolecular Chemistry and New Polymeric Materials, Zernike Institute for Advanced Materials, University of Groningen, Nijenborgh 4, 9747AG, Groningen, the Netherlands

ARTICLE INFO

Keywords:
Dielectric nanocomposites
Relaxor ferroelectric
Block copolymer
Selective dispersion
Hafnium oxide

ABSTRACT

The development of light and flexible capacitive energy storage devices with high electrical energy densities is of crucial significance to respond to the ever-rising demands in advanced applications and electricity needs. Incorporation of high dielectric constant ceramic fillers inside the ferroelectric polymer matrix offers great potential to improve the energy density of dielectric materials. However, this approach often suffers from highly reduced breakdown strength caused by the large difference of the matrix and filler dielectric constants together with often poor dispersion of the ceramic additives inside the polymer. Here, we demonstrate a simple method for the preparation of improved polymer-based dielectric nanocomposites based on self-assembly of medium dielectric constant hafnium oxide nanorods using ferroelectric block copolymer. The prepared nanocomposites exhibit both improved discharged energy densities and charge-discharge efficiencies, whereas they preserve their function up to comparable electric fields as the pristine block copolymer. The enhancement of the properties is mostly ascribed to the formation of deeper charge traps due to nanorod induced crosslinking inside amorphous domains and the reduction of ferroelectric loss influenced by creation of an additional paraelectric phase in nanocomposites.

1. Introduction

The development and ever-growing application of renewable solar, wind and biomass energy, caused by many ecological reasons and draining of the fossil fuel sources, have increased the need for advanced high efficiency electrical energy storage and conversion technologies [1]. Among current energy storage devices, electrostatic capacitors are unique for their high power density and ability to release stored energy in a short period of time (~microseconds), which makes them one of the primary candidates for storage and conversion of electrical energy [2,3]. The energy storage operation of capacitors is ascribed to their ability to separate opposite charges between two electrodes using an insulating dielectric material. However, the energy density values obtained using capacitors are low, causing them to occupy large volumes in electrical systems. As energy density is controlled by the choice of the dielectric material, the development of novel materials for charge separation displays the most promising approach to overcome this issue.

The stored energy density (U) of a dielectric capacitor is determined by the number of opposite charges separated by a dielectric material on two electrodes, as expressed by $U = \int EdD$, where E represents the applied electric field and D the electric displacement. Particularly for linear dielectrics, energy density scales linearly with the dielectric constant of dielectrics (ε_r) and quadratically with the applied electric field E, following the relation $U = 1/2\varepsilon_r\varepsilon_0E^2$, where ε_0 is the vacuum permittivity. Consequently, the ultimate goal is to create dielectric materials with both high dielectric constants and breakdown strength (E_b)–maximum electric fields that can be applied on the dielectric material.

Polymers are very attractive dielectric materials because of their easy processability, flexibility and low cost [4,5]. Additionally, they show low dielectric and conducting losses and high breakdown strength with a graceful failure mechanism [6,7]. In particular, ferroelectric polymers, such as poly(vinylidene fluoride), PVDF, and its copolymer with trifluoroethylene demonstrate high dielectric constant ($\varepsilon_r \sim 10$) and a large spontaneous polarization [8,9]. Their intrinsic high dielectric constant is closely related to the presence of C-F bonds with a

* Corresponding author.
E-mail address: k.u.loos@rug.nl (K. Loos).
[1] Both authors equally contributed to this work.

https://doi.org/10.1016/j.nanoen.2019.103939
Received 24 November 2018; Received in revised form 6 July 2019; Accepted 23 July 2019
Available online 25 July 2019

large dipole moment per monomeric unit (2.10 D) and their alignment in the PVDF β crystalline phase [10,11]. Unfortunately, this is the exact reason for the large remanent polarization and ferroelectric loss, which consequently decreases the charge-discharge efficiency of capacitors [12,13]. Nevertheless, the preparation of a poly(vinylidene fluoride-*co*-trifluoroethylene) with > 50 wt % of TrFE, poly(vinylidene fluoride-*ter*-trifluoroethylene-*ter*-chlorotrifluoroethylene) (PVDF-TrFE-CTFE) or poly(vinylidene fluoride-*ter*-trifluoroethylene-*ter*-chlorofluoroethylene) (PVDF-TrFE-CFE) results in the reduction of the ferroelectric loss, as the increased distance between crystalline planes and the formation of physical pinning spots, caused by the introduction of less polar bulkier monomers, allows easier dipole rotation with the applied electric field and therefore a near zero remanent polarization [14–17]. Additionally, these so called ferroelectric relaxor polymers possess the highest dielectric constant among all explored dielectric polymers, which makes them suitable for the application as high energy density dielectrics [18].

Recently, the preparation of polymer nanocomposites that consist of inorganic ceramic nano-objects dispersed in a ferroelectric polymer has arisen as an effective way to achieve improved polymer-based dielectrics [19–23]. The integration of nano-objects into the structure of ferroelectric polymers combines advantages of both components – a high dielectric constant of ceramics and high breakdown strength and flexibility of polymers. Even though it leads to the improvement of the material's dielectric constant, this approach is accompanied with serious issues that limit its viability. The low surface energy of ferroelectric polymers, induced by dense packing of fluorine atoms inside the crystalline phase, reduces their ability to mix with inorganic fillers, resulting in the formation of nanoparticle aggregates [11]. Additionally, low compatibility between a polymer and nano-objects drives the formation of defects and voids at the nano-object/polymer interface, which together increases conducting losses and failure at lower electric fields compared to the pure polymer [24–26]. Even with this problem solved, substantial differences in the dielectric constant between two phases develops regions in the polymer matrix near the interface where the electric field greatly surpasses the values of the applied electric field [27,28]. This uneven distribution of the electric field inside the material can significantly lower the breakdown strength. Having in mind a stronger influence of the applied electric field on the energy density compared to dielectric constant, the introduction of high dielectric constant fillers can conversely diminish energy density values. In addition to the above-mentioned issues, the orientation and selective distribution of nano-objects that can greatly alter the properties of nanocomposites, such as the breakdown strength, dielectric loss, electrical and thermal conductivity, are still considered as major challenges [29–34]. Most of the so far prepared and examined nanocomposites are established using the conventional blending of nano-objects with the polymer matrix without real control over their distribution [35,36].

In this contribution, we present an effective approach to address and overcome issues related to the preparation of dielectric polymer nanocomposites using a ferroelectric relaxor P2VP-*b*-P(VDF-TrFE)-*b*-P2VP block copolymer as a template to guide the dispersion of nano-objects (Scheme 1). The formation of strong hydrogen bonds between the surface of hafnium oxide nanorods and P2VP domains drives the selective homogeneous dispersion of ceramic nanorods inside lamellar domains made *via* the self-assembly process, whereas the medium dielectric constant of the filler prevents local distortions of the electric field. Applying this approach for the preparation of dielectric materials grants not only a homogeneous dispersion of nanoparticles but also reduced dielectric losses, improved discharged energy density and 34% improvement in the charge-discharge efficiency compared to the pristine block copolymer.

2. Experimental section

2.1. Materials

Trioctylphosphine oxide (TOPO) (> 95.0%, TCI Europe), hafnium (IV) isopropoxide (99%, Alfa Aesar), $HfCl_4$ (99%, Acros Organics) and gallic acid (98%, Acros Organics) were used as received. The block copolymer was prepared following literature procedure [40]. All solvents used for the film preparation and ligand exchange were analytical grade and used without further purification.

2.2. Synthesis of hafnium oxide nanorods

0.95 g (2 mmol) of hafnium(IV) isopropoxide and 0.65 g (2 mmol) of $HfCl_4$ were added to 10 g (25.9 mmol) of TOPO in a pre-dried triple neck flask under nitrogen atmosphere. The reaction mixture was heated fast to 360 °C, stirred for 2 h and subsequently cooled down to 60 °C. Nanocrystals are precipitated after addition of large amount of acetone followed by the centrifugation at 4500 rpm for 5 min. The precipitate was further washed five times with acetone and redispersed in tetrahydrofuran and passed through PTFE filter with 0.45 µm pore size. After additional precipitation of nanocrystals inside acetone, they were dispersed in tetrahydrofuran and stored in the fridge.

2.3. Ligand exchange

A solution of gallic acid in tetrahydrofuran (500 mg in 10 mL) was added drop-wisely inside 10 mL of 5 mg mL^{-1} solution of HfO_2 nanorods in tetrahydrofuran. To promote the ligand exchange, the obtained solution was kept in an ultrasonication bath overnight. The prepared nanorods were purified by precipitation with hexane and collected using centrifugation. The following procedure is repeated three times. Subsequently, the nanorods are dispersed in DMF at $c = 5$ mg mL^{-1} and kept in the fridge until further use.

2.4. Preparation of polymer films

The block copolymer was dissolved in 4 mL DMF (10 mg mL^{-1}) and the desired weight of nanoparticles was added. After passing through the 0.45 µm PTFE filter, the solution was cast in an aluminum pan (ø 30 mm). The solvent was allowed to evaporate at 45 °C over two days. Subsequently, the film was annealed at 170 °C for 5 min to induce the microphase separation. After cooling down and water lift-off, *ca.* 20 µm thick free-standing films were obtained.

2.5. Characterization

Small-angle X-ray scattering (SAXS) and Wide-angle X-ray scattering (WAXS) measurements were carried out at the Dutch-Belgium Beamline (DUBBLE) station BM26B of the European Synchrotron Radiation Facility (ESRF) in Grenoble, France, particularly optimized for polymer investigation [37–39]. The sample-to-detector distance was *ca.* 3.5 m for SAXS, *ca.* 28 cm for WAXS and an X-ray wavelength $\lambda = 0.97$ Å was used. SAXS images were recorded using a Pilatus 1 M detector while WAXS images were recorded using a Pilatus 100 KW detector, both with pixel size 172 × 172 µm x µm. The scattering angle scale was calibrated using the known peak position from a standard Silver Behenate sample. The scattering intensity is reported as a function of the scattering vector $q = 4\pi/\lambda(\sin\theta)$ with 2θ being the scattering angle and λ the wavelength of the X-rays. Deconvolution of the WAXS profiles was achieved using MATLAB. The experimental profiles were deconvoluted by using the sum of a linear background, and three pseudo-Voigt peaks describing the scattering from the amorphous and the two different crystalline phases. Transmission electron microscopy (TEM) of polymer films was performed on a Philips CM12 transmission electron microscope operating at an accelerating voltage of 120 kV. A

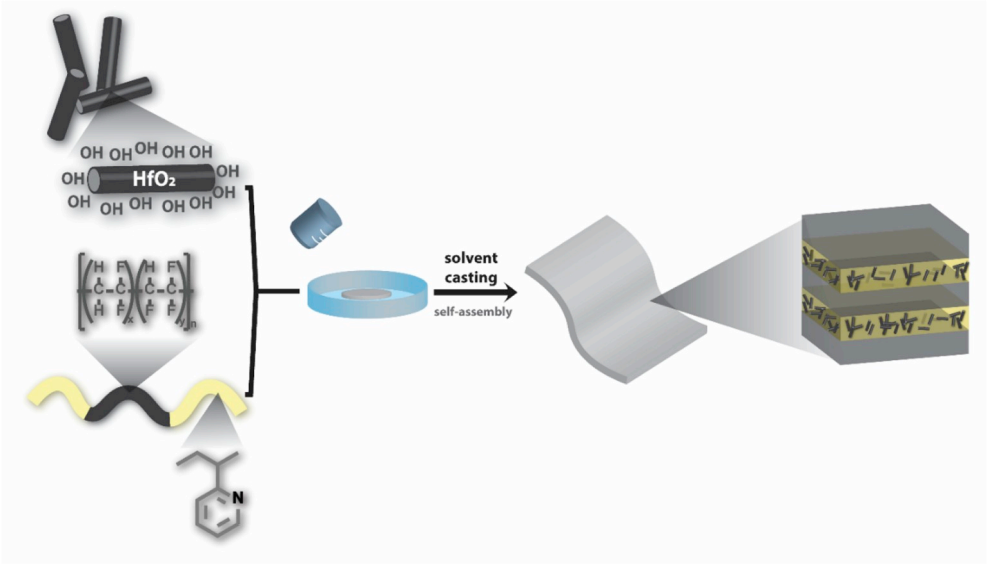

Scheme 1. Schematic representation of the block copolymer self-assembly method for the preparation of improved dielectric nanocomposites.

piece of film was embedded in epoxy resin (Epofix, Electron Microscopy Sciences) and microtomed using a Leica Ultracut UCT-ultramicrotome in order to prepare ultrathin sections (*ca.* 80 nm). Enhanced contrast for nanocomposite samples was achieved using iodine staining of thin sections for 40 min. Nanorod samples were prepared by drop-casting diluted NP solution in DMF onto carbon-supported copper grids. Fourier transform infrared (FTIR) spectra of hafnium oxide nanorods and gallic acid were recorded using a Bruker Vertex 70 spectrophotometer in ATR mode with 32 scans at a nominal resolution of 4 cm^{-1}. The unipolar D-E hysteresis measurements were performed using a state-of-the-art ferroelectric-piezoelectric tester aixACCT equipped with a Piezo Sample Holder Unit with a high voltage amplifier (0–10 kV). The AC electric field with a triangular wave form at frequency of 100 Hz was applied over polymer films immersed in silicon oil. The 100 nm thick gold electrodes (*ca.* 3.14 mm^2) with 5 nm chromium adhesion layer were evaporated onto both sides. DC conductivity of the polymer samples was obtained using the same equipment and same device configuration.

3. Results and discussion

In this study, a P2VP-*b*-P(VDF-TrFE)-*b*-P2VP block copolymer with 50 wt % of TrFE units is chosen as the polymer matrix for the preparation of nanocomposites. Recently, we have demonstrated the double loop, antiferroelectric-like-relaxor behavior in this polymer, caused by the existence of two crystalline phases (paraelectric and defective ferroelectric) [40]. The choice of the insulating P2VP block is made not only due to its relatively medium dielectric constant that does not strongly reduce the intrinsically high dielectric constant of the ferroelectric polymer, but also for the possibility to form strong hydrogen bonds with various hydrogen donors [41–43]. The block copolymer is synthesized using a copper catalyzed azide/alkyne cycloaddition reaction applied to the azide terminated P(VDF-TrFE) prepared using a free radical copolymerization of VDF and TrFE in the presence of a chlorine functionalized benzoyl peroxide initiator and alkyne terminated P2VP obtained via reversible addition-fragmentation chain transfer (RAFT) polymerization [44–47]. Such a facile method for the block copolymer synthesis, which relies on the chemical bonding of pre-synthesized building blocks, allows straightforward variation of the length, block ratio and consequently the morphology of block copolymers. However, we directed our attention to a particular block copolymer with M_n = 34.3 kg mol^{-1}, *PDI* = 1.72 and 30 wt % of P2VP units (Figs. S1 and S2) [40]. This block copolymer displayed a strong phase separation in the melt forming a lamellar morphology with a P2VP layer thickness comparable in size to the length of the synthesized hafnium oxide nanorods, which improves the probability for a successful dispersion of nanorods inside P2VP layers.

Hafnium oxide presents a wide bandgap electrical insulator with a dielectric constant of 22 [48]. Rod-shaped hafnium oxide nanofillers are synthesized through the nonhydrolytic sol-gel condensation route developed by Tang and co-workers [49]. This simple preparation method is based on the condensation of hafnium isopropoxide and hafnium chloride with the elimination of isopropyl chloride in the presence of stabilizing trioctylphosphine oxide (TOPO). Fig. 1a and b show a corresponding transmission electron microscopy (TEM) image of the obtained nanocrystals together with the length and width size distribution histograms. This synthetic procedure results in highly monodisperse 2.2 ± 0.4 nm thin nanorods and average length of 10.6 ± 2.5 nm, demonstrating the anisotropic growth of the crystals. The crystalline structure is determined according to the XRD pattern of the as-synthesized nanorods (Fig. 1c). The XRD pattern is in agreement with that of monoclinic HfO_2 with a particularly narrow and intense (200) reflection, suggesting preferential growth of nanocrystals in (100) direction, as confirmed with TEM.

Since the sol-gel reaction occurs in the presence of a non-polar TOPO, the surface of nanorods - directly after synthesis - is covered with long alkyl chains that prevent their good dispersion in polar solvents and P2VP layers. Therefore, an effective ligand exchange process is performed to replace the original ligands with gallic acid, able to form strong interactions with P2VP monomer units [50,51]. In addition to multiple groups that can form hydrogen bonds with P2VP and help to achieve better dispersion of nanorods, the presence of carbonyl and three hydroxyl groups with a high dipole moment can be beneficial for preparing nanocomposites with an improved dielectric constant [52]. Additionally, the application of less polar ligands would result in the distortion of the local electric field at the nanoparticle-polymer interface and significantly reduce the breakdown strength of the nanocomposites. The obtained nanorods demonstrate excellent dispersibility in many polar solvents, especially in *N,N*-dimethylformamide (no aggregation is observed even after one year), due to the hydrogen bond formation between the ligands on the nanorod's surface and the solvent molecules. The shift of the C = O stretching vibration signal of the gallic acid on the hafnium oxide nanorods from 1605 cm^{-1} to 1652 cm^{-1} observed in Fig. 1d suggests that the carboxylic group of the ligand is

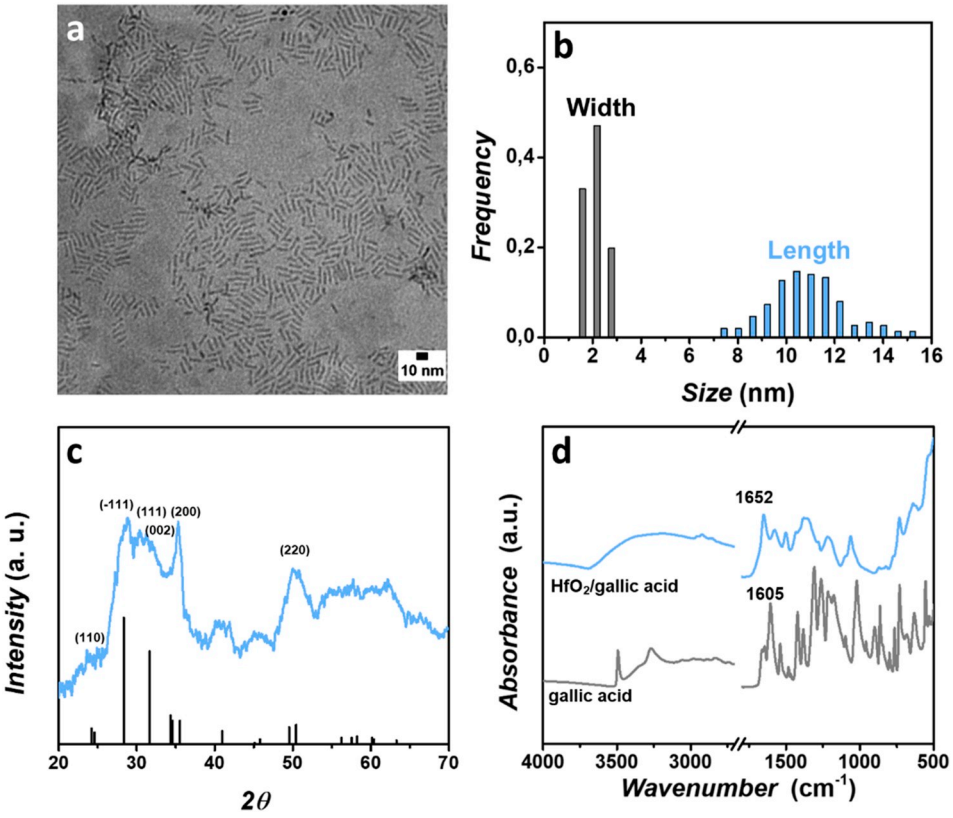

Fig. 1. (a) TEM micrograph of the gallic acid hafnium oxide nanorods cast from DMF. (b) The average length of the nanorods is 10.6 ± 2.5 nm, whereas the width is 2.2 ± 0.4 nm. Both values are obtained using ImageJ image analysis of 150 nanorods. (c) XRD pattern of the hafnium oxide nanorods. The pattern is indexed to the monoclinic phase of HfO_2. (d) The FTIR spectra of gallic acid and nanorods functionalized with gallic acid demonstrating a successful ligand exchange and bond formation between the surface of the nanorods and gallic acid.

mostly interacting with the nanorod surface.

Polymer nanocomposite films are prepared via a simple solution casting technique. The block copolymer solution in DMF with different content of gallic acid coated nanorods is casted in an aluminum Petri dish at 45 °C for two days. The polymer films are subsequently heated to 170 °C and kept for 5 min to induce microphase separation. Cooling down nanocomposite samples and pealing them off from the substrate using the water lift-off technique results in *ca.* 20 μm thick free-standing films. It is important to note that the use of the P(VDF-TrFE) with the same molecular weight as the one used for the block copolymer preparation gives extremely brittle films that cannot be used in further electrical measurements. This just demonstrate the beneficial effect of block copolymer preparation on the film formation ability, crucial for dielectric nanocomposites.

The morphology of the prepared nanocomposites is investigated using small-angle X-ray scattering (SAXS), complemented by TEM [37,38]. As shown in Fig. 2a, the SAXS profile of the pristine block copolymer shows a sharp primary peak centered at 0.18 nm^{-1} with two additional higher order peaks with ratios $1q^*$: $2q^*$: $3q^*$, indicative of a lamellar phase with average spacing $d_L = 2\pi/q^* = 34$ nm. The lamellar morphology is furthermore confirmed by TEM, as depicted in Fig. 2c, where the dark layers correspond to the crystalline P(VDF-TrFE) and the light layers belong to the amorphous P2VP. The quality of the nanorod dispersion inside the block copolymer is examined using the TEM of the microtomed samples. Fig. 2d–f show a uniform and selective dispersion of nanorods inside the P2VP domains of the block copolymer. Compared to a pristine block copolymer, P2VP layer appears dark, due to staining with iodine.

The spatial distribution of nano-objects in block copolymers is a consequence of the relationship between the conformational entropy of polymer chains, translational entropy of nano-objects and enthalpy caused by the creation of the polymer nano-object interface [53]. The entropy loss related to the insertion of nano-objects is dictated by their size and block copolymer domains, while the interaction between polymer chains and nano-objects determines the enthalpy of insertion [54]. The important feature of block copolymer nanocomposites is the selective dispersion of nano-objects, where they tend to localize in one of the domains formed by the self-assembly. The localization of nano-objects is mostly governed by the size, concentration and their surface functionalization. Small nanorods often localize at the interface between blocks, since the gain in translational entropy prevails over the loss in the conformational entropy of polymer chains after the nanoparticle incorporation. Conversely, the loss in conformational entropy is a dominant factor for the dispersion of larger nano-objects, which leads to their localization in the interior of polymer domains [55]. Nevertheless, the surface chemistry of nano-objects has the strongest influence on their specific localization inside block copolymer nanodomains, and can be tuned by the type, grafting density and molecular weight of the ligand [51].

The nanorod localization in the P2VP layer results from the favorable hydrogen bond formation between functional groups of ligand molecules and the nitrogen in the pyridine ring, consistent with the previous reports of the selective nano-object distribution inside block copolymers [56,57]. The existence of crystalline domains in the block copolymer helps the selective dispersion of nanorods inside amorphous layers, since nanorods are excluded due to crystallization of the P(VDF-TrFE) segments [57]. Both factors together are responsible for the absence of macrophase separation at high nanorod concentrations, as well as the formation of only small isolated aggregate clusters, still located in the P2VP phase. The confinement of nanorods inside the two-dimensional lamellar space did not result in a specific orientation of the nanorods. The conformation with all nanorods oriented parallel to the lamella plane induces a minimal deformation of polymer chains, and would be preferable for block copolymer-nanorod composites. However, the presence of small nanorods, with both the width and length smaller than the P2VP layer thickness has no significant effect on the conformational entropy of polymer chains. This, together with the strong enthalpic contribution from the hydrogen bonding between nanorods and polymer chains, causes the random orientation of nanorods. As expected, the selective incorporation of the nanorods inside the

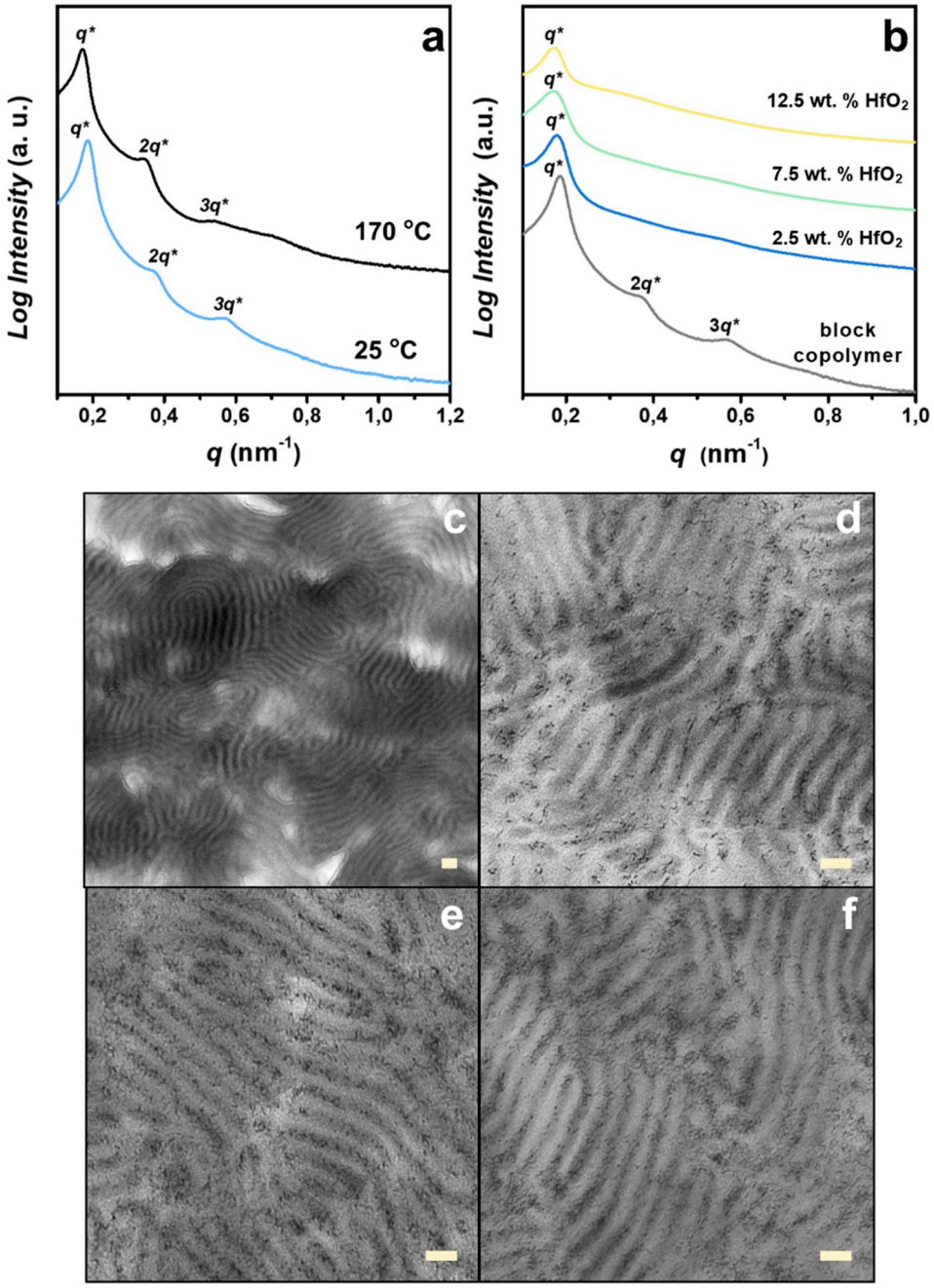

Fig. 2. (a) SAXS profile for a block copolymer collected at 170 °C and at room temperature showing the formation of the lamellar structure in the melt and confined crystallization inside lamellar domains. (b) SAXS profiles of block copolymer and nanocomposites at different loading of nanorods. TEM images of (c) pristine block copolymer and nanocomposites with (d) 2.5 wt %, (e) 7.5 wt %, (f) 12.5 wt % of hafnium oxide nanorods. Compared to a pristine block copolymer, P(VDF-TrFE) appears light, due to staining with iodine. The scale bars correspond to 50 nm.

P2VP blocks results in the increase of the lamellar domain spacing from 34 nm for the pristine block copolymer to 38 nm (Fig. 2b). No significant influence of the hafnium oxide incorporation on the structure of the block copolymer has been observed, independently of the nanorod concentration used. In all cases, a lamellar morphology is obtained, as demonstrated by TEM.

Differential scanning calorimetry (DSC) and wide-angle X-ray scattering (WAXS) measurements are carried out to examine the effect of the nanorod incorporation on the crystalline structure of the nanocomposites [39]. As observed in the cooling DSC profiles (Fig. S3), the crystallization temperature (T_c) in similar for all samples. Additionally, the crystallization enthalpy related to the P(VDF-TrFE) block increases only slightly from 12.7 J g^{-1} for the pristine block copolymer to 13.4 J g^{-1} for the nanocomposites, probably caused by the improved phase segregation strength between the blocks. Nevertheless, the overall crystallinity of the sample, which strongly influences the ferroelectric response, slightly decreases with the addition of nanorods, since the content of the crystalline block inside the block copolymer reduces.

The WAXS of the neat block copolymer demonstrates two crystalline phases present inside the material (Fig. 3a). The reflection located at 13.5 nm^{-1} agrees with the cooled ferroelectric phase (CLFE) with mainly trans conformation with few gauche defects and a high temperature paraelectric phase (HTPE) at 13.1 nm^{-1} [58]. The same crystalline phases are found for all nanocomposites regardless of the nanorod concentration. However, the incorporation of the filler inside

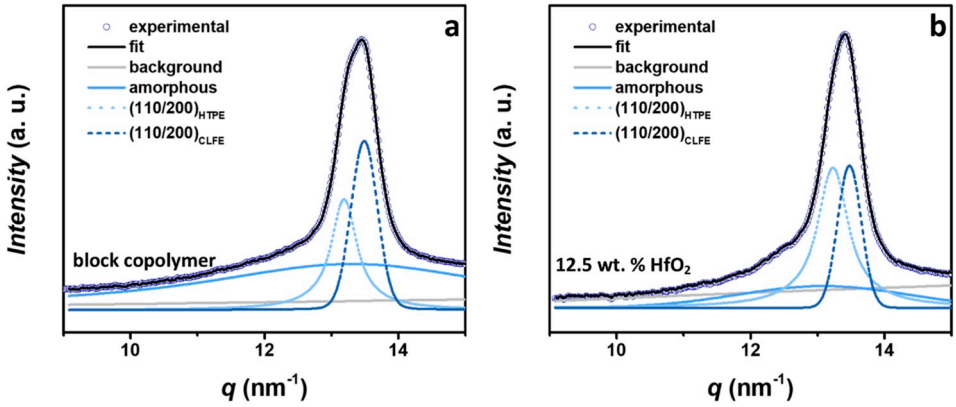

Fig. 3. WAXS profiles of (a) the pristine block copolymer and (b) the nanocomposite with 12.5 wt % of HfO_2. The addition of the nanorods causes an increase in the content of the high temperature paraelectric phase.

Table 1
Crystalline properties of the block copolymer and nanocomposites.

Sample name	ΔH_c [a] (J g^{-1})	ΔH_c' [b] (J g^{-1})	T_c [c] (^{0}C)	% of HTPE [d]
block copolymer (BCP)	8.9	12.7	127	48.5
BCP/2.5 wt % HfO_2	8.9	13.0	128	60.5
BCP/7.5 wt % HfO_2	8.7	13.4	128	59.8
BCP/12.5 wt % HfO_2	8.3	13.4	127.5	65.0

[a] Determined using DSC and related to the weight of the whole sample.
[b] Calculated related to the weight fraction of the crystalline P(VDF-TrFE) block.
[c] Determined using DSC.
[d] Calculated from WAXS after deconvolution of the crystalline peak. The corresponding values are relative to the total crystalline content.

the block copolymer induces changes in the relative content of the existing crystalline phases. As shown in Table 1 and Fig. 3b, with the addition of hafnium oxide nanorods to the P2VP layer, the amount of the high temperature paraelectric phase increases compared to the cooled ferroelectric phase. Interestingly, no difference in the paraelectric phase content exists between nanocomposites with 2.5 and 7.5 wt % of hafnium oxide, while the subsequent increase in their concentration induces an additional rise in the amount of the paraelectric phase. It is well known that the addition of fillers and the subsequent hydrogen bond induced crosslinking of the matrix generates a more rigid structure of the polymer matrix and improves phase separation between the blocks [57]. This results in a more pronounced stretching of the crystalline block at the interface and less effect of the amorphous layers on the mobility of the crystallizable block in the melt. Thus, the crystalline block is more prone to crystallize in the defect-free paraelectric phase. The additional increase in the paraelectric phase at a high concentration of nanorods can be explained by the effect of the nanorod surface on the crystallization mechanism. The nanoparticle migration to the crystalline layers occurs at a high content of a nanofiller, which considering the polar surface of nanorods can induce the formation of the paraelectric phase [59,60].

Fig. 4b and c reveal the D-E loops for the pristine block copolymer and nanocomposite with 12.5 wt % nanorods measured at different electric fields with a 100 Hz unipolar triangular signal (Fig. 4a). From the shape of the D-E loops the polarization saturation characteristic of ferroelectric polymers can be observed. Compared to the pristine block copolymer, the nanocomposite shows distinctly slimmer loops with the reduced remanent displacement at examined electric fields. Taking into consideration the reduced overall amount of the ferroelectric block inside the nanocomposite, one would expect a gradual decrease of the maximum displacement with the increase of the nanorod content. However, both samples demonstrate no difference at the same fields. The increase of displacement with the addition of nanofillers is reported to be associated with interface effects [23,36]. Since the good dispersion of ultra-small nanorods is achieved using strong hydrogen bonding, a large interfacial area exists between nanorods and the polymer matrix and it is responsible for a Maxwell-Wagner-Sillars (MWS) interfacial polarization [35]. Therefore, the addition of well dispersed nano-object results in increased displacement, which together with the reduction of the ferroelectric component content gives the unaltered maximum displacement for the nanocomposite compared to the pristine block copolymer.

The value of the remanent displacement is a direct consequence of the dielectric loss at high fields in a material, that for ferroelectrics origins both from the electrical conduction and the spontaneous polarization of dipoles. It is evident that the remanent displacement decreases systematically with the content of hafnium oxide inside the material (from 0.71 μC cm^{-1} of the neat block copolymer to 0.39 μC cm^{-1} of nanocomposite with 12.5 wt % of hafnium oxide at 275 MV m^{-1}) where this difference becomes particularly obvious at higher electric fields (Fig. 4d). This is in agreement with the results obtained from nanocomposites containing fillers with high breakdown strength and a lower or comparable dielectric constant than the polymer matrix [21,22]. The presence of clear convex regions on the D-E loop of the pristine block copolymer at high fields, typical for a lossy dielectric, indicates the main influence of conductive losses on the overall losses in the material. Indeed, as demonstrated in Fig. 4e, the gradual reduction of the DC conductivity occurs with the increased content of nanorods. The nanocomposite sample with 12.5 wt % of nanorods shows one order of magnitude lower conductivity compared to the pristine block copolymer. This is somewhat expected due to the very low conductivity of hafnium or similar oxides (ZrO_2 or Ta_2O_5), as low as 10^{-14} S m^{-1}, which is even below the values of the block copolymer [48]. Moreover, the addition of nanorods inside P2VP layers and the strong hydrogen bonding cause a physical crosslinking of the polymer matrix surrounding the nanorods. The crosslinking of the P2VP domains constrains the chain mobility in amorphous regions, which as a consequence leads to the formation of deeper traps in the regions around the nanorods [61]. In addition, the surface of the hafnium nanorods is covered with hydroxyl groups, which are well known to act as electron traps that reduce their conduction [62]. Having in mind that not all functional groups on the surface of the hafnium oxide nanorods are consumed in the hydrogen bond formation, it is expected that these groups additionally suppress the mobility of charge carriers. In addition to the lower conductivity of nanocomposites, the increased content of the paraelectric phase compared to the neat block copolymer additionally reduces dielectric losses. After the removal of the electric field, the dipoles of the paraelectric field are able to relax and return back into their unoriented state, which improves the switchability and

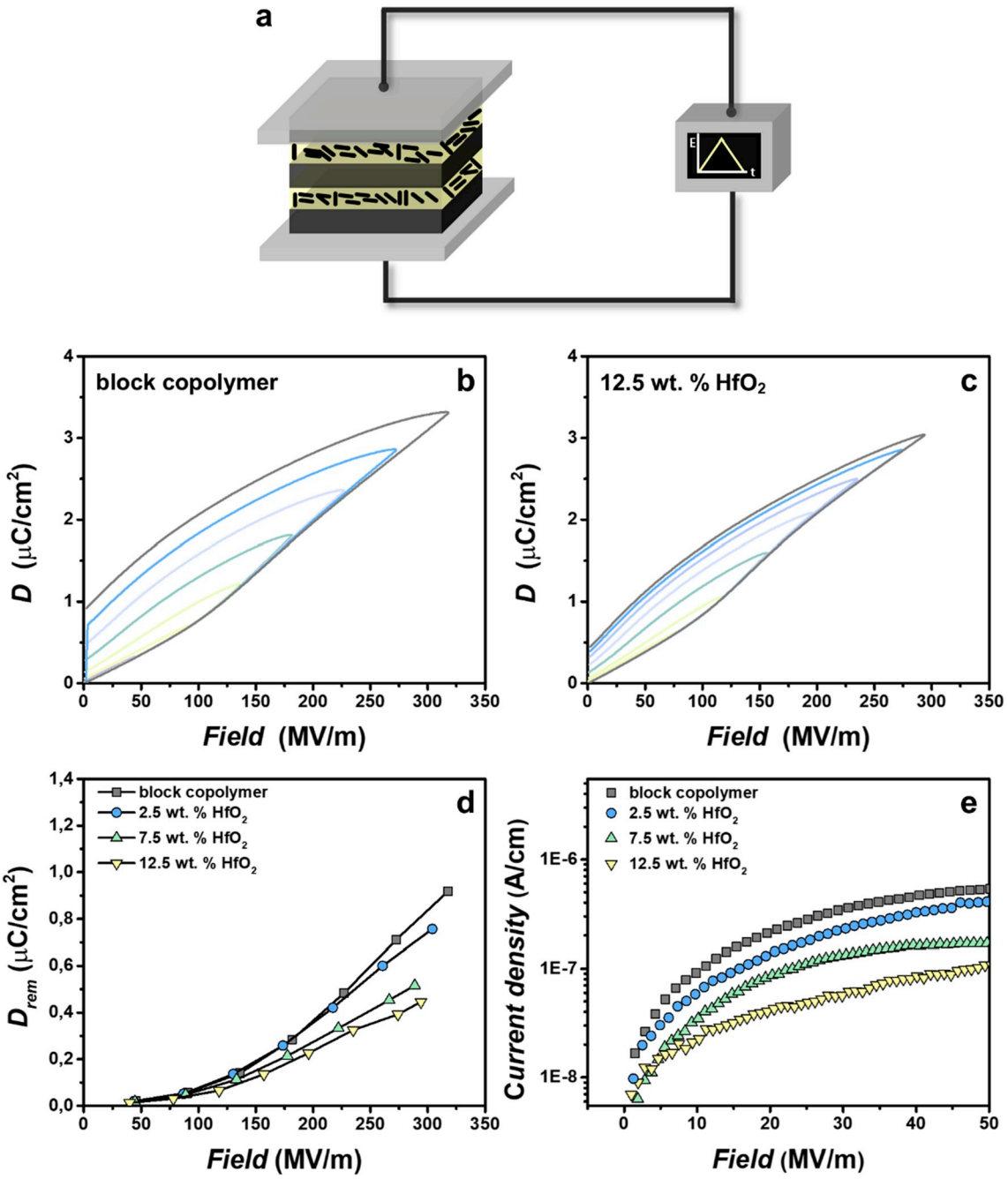

Fig. 4. (a) Experimental setup for the measurement of the D-E loops used for the calculation of the energy density values. Unipolar D-E loops of (b) the pristine block copolymer and (c) the nanocomposite with 12.5 wt % of HfO_2. (d) Influence of the nanorod content on the remanent displacement of the dielectrics at different electric field values. (e) The dependence of DC current density on the applied electric field for different content of nanorods inside the block copolymer.

reduces ferroelectric losses.

The discharged energy density (U_d) values are determined form the D-E loops (Fig. 5a) by integrating the areas between the discharge curve and the ordinate, as depicted in the onset of Fig. 5b. As shown in Fig. 5a, the discharged energy density of the pristine block copolymer is 2.3 J cm^{-3} at 275 MV m^{-1}, whereas nanocomposite with 12.5 wt % of nanorods release 2.8 J cm^{-3} at the same field, which is 2.8 times improvement compared to the currently used biaxially oriented polypropylene (U_d = 1.0 J cm^{-3} at 275 MV m^{-1}) [7]. This clearly demonstrates the beneficial effect of a good dispersion of medium dielectric constant nanorods inside the polymer matrix on the amount of energy that can be obtained from the material after storage. It is important to underline that the prepared nanocomposites can withstand comparable electric fields as the pristine block copolymer and noticeably higher than the nanocomposites prepared in a conventional way using high dielectric constant fillers $BaTiO_3$, TiO_2 or metal nanoparticles. The presence of nanorods with the comparable dielectric constant as the polymer matrix generates a more even electric field distribution in a material, without interfacial regions with drastically increased electric field values. This, together with the low conductivity of the filler enables nanocomposites to operate at relatively high fields. Moreover, the high polarity of the P2VP layers compared to the crystalline P(VDF-TrFE) induces the preferential orientation of lamellar domains at the contact with aluminum and air, parallel to the interface (Fig. S5). In this way, the formation of conducting pathways is hindered, which prevents a premature breakdown. However, with this configuration of the

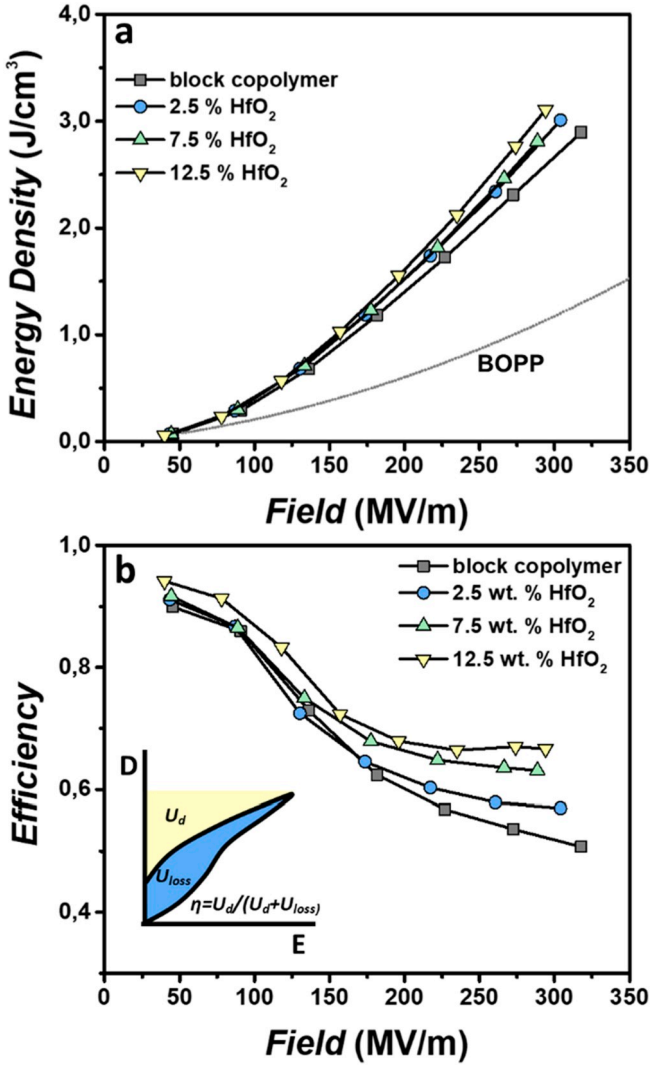

Fig. 5. (a) The discharged energy density of the block copolymer and nanocomposites with a different content of HfO_2 nanorods calculated from unipolar D-E loops. The released energy density values of the state-of-the-art BOPP are included for comparison purposes (data extrapolated from Ref. [7]. (b) The dependence of charge-discharge efficiency on the applied electric field for a different content of nanorods inside the block copolymer.

dielectric material, one would expect nanocomposites to operate at higher fields compared to the pristine block copolymer. The probable reason for the absence of this phenomenon lays in the redistribution of the electric fields between lamellar layers after the incorporation of the nanorods [28]. As the nanorods pose higher permittivity than the P2VP, their addition will result in an increase of the amorphous layer dielectric constant. As a consequence, the nominative electric field that senses the crystalline layer will be larger than for the pristine block copolymer, which can possibly result in an earlier breakdown of nanocomposite samples than expected.

Another property that defines the performance of dielectric materials is their charge-discharge efficiency (η) (Fig. 5b). The unreleased energy produces heat inside the material and has a detrimental effect on the durability of dielectrics. It is important to note that the charge-discharge efficiency of the pristine block copolymer is relatively low at high field (53% at 275 MV m^{-1}). The low efficiency is a characteristic of ferroelectric polymers and it is attributed to their large hysteresis and a consequent ferroelectric loss due to the formation of crystalline domains with oriented dipoles. Even though the block copolymer used for the nanocomposite preparation demonstrates relaxor behavior, ferroelectric losses are still unavoidable. However, the nanocomposites demonstrate fairly higher charge–discharge efficiencies, which is a result of the reduced dielectric loss at high electric fields. As an illustration, the incorporation of 12.5 wt % of hafnium oxide nanorods increases the efficiency values to 67%, a 34% improvement over the pristine block copolymer.

4. Conclusion

In summary, we have established a straightforward method for the preparation of solution-processed dielectric nanocomposites based on the selective dispersion of nanofillers inside relaxor ferroelectric block copolymers. It is found that the formation of strong hydrogen bonds between surface modified hafnium oxide nanorods and the P2VP block provides the preferential dispersion of nanorods inside amorphous domains without aggregation. The prepared organic-inorganic nanostructured composite materials demonstrate reduced mobility of charge carriers through the material and consequently lower dielectric losses. The formation of the physically crosslinked network in the amorphous regions, together with the formation of the additional paraelectric phase after the nanofiller addition is responsible for the improved discharged energy density and charge-discharge efficiency of nanocomposites and their ability to operate at comparable electric fields as the pristine polymer. Unfortunately, the energy density values obtained with the prepared materials are far from the desired values for final applications. However, a vast range of design manipulations is possible to implement using the block copolymer approach to improve and achieve the ultimate performance of nanocomposites. Improved material response could be achieved by increasing the orientation of lamellar domains, by increasing of the molecular weight of the polymer, by the adjustment of the size, shape and type of the nanofiller, by controlling the structure of the ferroelectric and amorphous blocks, and by varying the ratio between blocks and the morphology of nanocomposites. Given the large room for improvement, even though just demonstrated as a proof-of-concept example, the approach illustrated in this work represents a promising and simple method for the development of future polymer-based dielectrics.

Notes

The authors declare no competing financial interest.

Acknowledgements

This work was supported by the Netherlands Organisation for Scientific Research (NWO) via a VICI innovational research grant. The authors are very grateful to Prof. Beatriz Noheda and Mónica Acuautla for the valuable discussion regarding the ferroelectric measurements, and Dina Maniar for help preparing images in this manuscript and XRD measurements of nanorods. NWO and the ESRF are acknowledged for granting the beamtime at DUBBLE. Daniel Hermida-Merino is acknowledged for his experimental assistance with the synchrotron experiments.

Appendix A. Supplementary data

Supplementary data to this article can be found online at https://doi.org/10.1016/j.nanoen.2019.103939.

References

[1] E. Karden, S. Ploumen, B. Fricke, T. Miller, K. Snyder, J. Power Sources 168 (2007) 2.
[2] S. Ducharme, ACS Nano 3 (2009) 2447.
[3] G.R. Love, J. Am. Ceram. Soc. 73 (1990) 323.
[4] Z.-M. Dang, J.-K. Yuan, S.-H. Yao, R.-J. Liao, Adv. Mater. 25 (2013) 6334.
[5] B. Chu, X. Zhou, K. Ren, B. Neese, M. Lin, Q. Wang, F. Bauer, Q.M. Zhang, Science

313 (2006) 334.
[6] L. Zhu, J. Phys. Chem. Lett. 5 (2014) 3677.
[7] S. Wu, W. Li, M. Lin, Q. Burlingame, Q. Chen, A. Payzant, K. Xiao, Q.M. Zhang, Adv. Mater. 25 (2013) 1734.
[8] A.J. Lovinger, Science 220 (1983) 1115.
[9] H.S. Nalwa, Ferroelectric Polymers: Chemistry, Physics, and Applications, M. Dekker, Inc, New York , 1995.
[10] F. Guan, J. Wang, J. Pan, Q. Wang, L. Zhu, Macromolecules 43 (2010) 6739.
[11] B. Ameduri, Chem. Rev. 109 (2009) 6632.
[12] M. Panda, AIP Conf. Proc. 1953 (2018) 020001.
[13] G. Liu, S. Zhang, W. Jiang, W. Cao, Mater. Sci. Eng. R Rep. 89 (2015) 1.
[14] T. Furukawa, A.J. Lovinger, G.T. Davis, M.G. Broadhurst, Macromolecules 16 (1983) 1885.
[15] M.R. Gadinski, Q. Li, G. Zhang, X. Zhang, Q. Wang, Macromolecules 48 (2015) 2731.
[16] L. Yang, B.A. Tyburski, F.D. Dos Santos, M.K. Endoh, T. Koga, D. Huang, Y. Wang, L. Zhu, Macromolecules 47 (2014) 8119.
[17] Y. Liu, H. Aziguli, B. Zhang, W. Xu, W. Lu, J. Bernholc, Q. Wang, Nature 562 (2018) 96.
[18] Y. Lu, J. Claude, B. Neese, Q. Zhang, Q. Wang, J. Am. Chem. Soc. 128 (2006) 8120.
[19] J. Li, J. Claude, L.E. Norena-Franco, S.I. Seok, Q. Wang, Chem. Mater. 20 (2008) 6304.
[20] L. Xie, X. Huang, K. Yang, S. Li, P. Jiang, J. Mater. Chem. A 2 (2014) 5244.
[21] Q. Li, G. Zhang, F. Liu, K. Han, M.R. Gadinski, C. Xiong, Q. Wang, Energy Environ. Sci. 8 (2015) 922.
[22] K. Han, Q. Li, C. Chanthad, M.R. Gadinski, G. Zhang, Q. Wang, Adv. Funct. Mater. 25 (2015) 3505.
[23] Prateek, V.K. Thakur, R.K. Gupta, Chem. Rev. 116 (2016) 4260.
[24] Q. Wang, L. Zhu, J. Polym. Sci. Part B Polym. Phys. 49 (2011) 1421.
[25] T. Zhou, J.-W. Zha, R.-Y. Cui, B.-H. Fan, J.-K. Yuan, Z.-M. Dang, ACS Appl. Mater. Interfaces 3 (2011) 2184.
[26] X. Zhang, B.-W. Li, L. Dong, H. Liu, W. Chen, Y. Shen, C.-W. Nan, Adv. Mater. Interfaces 5 (2018) 1800096.
[27] Z.-H. Shen, J.-J. Wang, Y. Lin, C.-W. Nan, L.-Q. Chen, Y. Shen, Adv. Mater. 30 (2018) 1704380.
[28] J. Kuffel, P. Kuffel, High Voltage Engineering Fundamentals, Elsevier, 2000.
[29] D. Zhang, W. Liu, R. Guo, K. Zhou, H. Luo, Adv. Sci. 5 (2018) 1700512.
[30] B. Li, P.I. Xidas, E. Manias, ACS Appl. Nano Mater. 1 (2018) 3520.
[31] J.-P. Cao, X. Zhao, J. Zhao, J.-W. Zha, G.-H. Hu, Z.-M. Dang, ACS Appl. Mater. Interfaces 5 (2013) 6915.
[32] V.S.D. Voet, K. Kumar, G. ten Brinke, K. Loos, Macromol. Rapid Commun. 36 (2015) 1756.
[33] V.S.D. Voet, M. Tichelaar, S. Tanase, M.C. Mittelmeijer-Hazeleger, G. ten Brinke, K. Loos, Nanoscale 5 (2013) 184.
[34] V.S.D. Voet, D. Hermida-Merino, G. ten Brinke, K. Loos, RSC Adv. 3 (2013) 7938.
[35] J. Li, P. Khanchaitit, K. Han, Q. Wang, Chem. Mater. 22 (2010) 5350.
[36] J. Li, S.I. Seok, B. Chu, F. Dogan, Q. Zhang, Q. Wang, Adv. Mater. 21 (2009) 217.
[37] M. Borsboom, W. Bras, I. Cerjak, D. Detollenaere, D. Glastra van Loon, P. Goedtkindt, M. Konijnenburg, P. Lassing, Y.K. Levine, B. Munneke, M. Oversluizen, R. van Tol, E. Vlieg, J. Synchrotron. Rad. 5 (1998) 518.
[38] W. Bras, I.P. Dolbnya, D. Detollenaere, R. van Tol, M. Malfois, G.N. Greaves, A.J. Ryan, E. Heeley, J. Appl. Crystallogr. 36 (2003) 791.
[39] G. Portale, D. Cavallo, G.C. Alfonso, D. Hermida-Merino, M. van Drongelen, L. Balzano, G.W.M. Peters, J.G.P. Goossens, W. Bras, J. Appl.Cryst. 46 (2013) 1681.
[40] I. Terzic, N.L. Meereboer, M. Acuautla, G. Portale, K. Loos, Nat. Commun. 10 (2019) 601.
[41] S. Bondzic, J. de Wit, E. Polushkin, A.J. Schouten, G. ten Brinke, J. Ruokolainen, O. Ikkala, I. Dolbnya, W. Bras, Macromolecules 37 (2004) 9517.
[42] A.H. Hofman, I. Terzic, M.C.A. Stuart, G. ten Brinke, K. Loos, ACS Macro Lett. 1168 (2018).
[43] M. Golkaram, C. Fodor, E. van Ruymbeke, K. Loos, Macromolecules 51 (2018) 4910.
[44] I. Terzic, N.L. Meereboer, K. Loos, Polym. Chem. 9 (2018) 3714.
[45] N.L. Meereboer, I. Terzić, S. Saidi, D. Hermida Merino, K. Loos, ACS Macro Lett. (2018) 863.
[46] V.S.D. Voet, G.O.R.A. van Ekenstein, N.L. Meereboer, A.H. Hofman, G. ten Brinke, K. Loos, Polym. Chem. 5 (2014) 2219.
[47] V.S.D. Voet, G. ten Brinke, K. Loos, J. Polym. Sci. Part A Polym. Chem. 52 (2014) 2861.
[48] J. Robertson, Eur. Phys. J. Appl. Phys. 28 (2004) 265.
[49] J. Tang, J. Fabbri, R.D. Robinson, Y. Zhu, I.P. Herman, M.L. Steigerwald, L.E. Brus, Chem. Mater. 16 (2004) 1336.
[50] X. Wang, R.D. Tilley, J.J. Watkins, Langmuir 30 (2014) 1514.
[51] Y. Gai, Y. Lin, D.-P. Song, B.M. Yavitt, J.J. Watkins, Macromolecules 49 (2016) 3352.
[52] Z.-H. Dai, J.-R. Han, Y. Gao, J. Xu, J. He, B.-H. Guo, Colloid. Surf. Physicochem. Eng. Asp. 529 (2017) 560.
[53] V. Pryamitsyn, V. Ganesan, Macromolecules 39 (2006) 8499.
[54] H. Kang, F.A. Detcheverry, A.N. Mangham, M.P. Stoykovich, K.C. Daoulas, R.J. Hamers, M. Müller, J.J. de Pablo, P.F. Nealey, Phys. Rev. Lett. 100 (2008) 148303.
[55] M.R. Bockstaller, Y. Lapetnikov, S. Margel, E.L. Thomas, J. Am. Chem. Soc. 125 (2003) 5276.
[56] L. Yao, Y. Lin, J.J. Watkins, Macromolecules 47 (2014) 1844.
[57] Y. Lin, X. Wang, G. Qian, J.J. Watkins, Chem. Mater. 26 (2014) 2128.
[58] A.J. Lovinger, G.T. Davis, T. Furukawa, M.G. Broadhurst, Macromolecules 15 (1982) 323.
[59] I. Terzic, N.L. Meereboer, H.H. Mellema, K. Loos, J. Mater. Chem. C 7 (2019) 968.
[60] N.L. Meereboer, I. Terzic, H.H. Mellema, G. Portale, K. Loos, Macromolecules 52 (2019) 1567.
[61] P. Khanchaitit, K. Han, M.R. Gadinski, Q. Li, Q. Wang, Nat. Commun. 4 (2013) 2845.
[62] S. Lee, B. Koo, J. Shin, E. Lee, H. Park, H. Kim, Appl. Phys. Lett. 88 (2006) 162109.

Niels Meereboer was born in Warmenhuizen, the Netherlands, in 1988. He received his B.Sc (2011) and M.Sc. (2014) degrees in Polymer Chemistry from the University of Groningen. Now he is a Ph.D. candidate under the supervision of Professor Katja Loos. His research interest focuses on designing, synthesizing, processing and characterizing fluorinated polymers for capacitive energy storage applications.

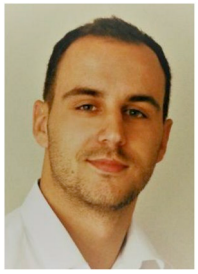

Ivan Terzić received B.Sc (2013) and M.Sc. (2014) degrees in Polymer Engineering form the University of Belgrade. He is currently a Ph.D. candidate in the Macromolecular Chemistry and New Polymeric Materials group at University of Groningen. His research interests include design, synthesis, self-assembly and characterization of ferroelectric block copolymers and their nanocomposites.

Giuseppe Portale graduated and received his Ph.D in chemistry from the University of Rome "La Sapienza". After a Ph.D., he moved to the ESRF for a post-doc funded by the Dutch Polymer Institute in 2006 to develop new experiments to study polymer structure and dynamics with X-rays. In 2009 he became beam line scientist for the Netherlands Organization for Scientific Research at the ESRF, where he was the responsible for the SAXS/WAXS BM26B beam line. From 2015, he is Assistant Professor at the Zernike Institute for Advanced Materials in Groningen where he leads the group of polymer physics with focus on the structure-property relationships in polymers for energy applications and in organic/inorganic hybrid systems.

Katja Loos is Professor at the Zernike Institute for Advanced Materials of the University of Groningen, The Netherlands holding the chair of Macromolecular Chemistry and New Polymeric Materials. She specialized in Organic Chemistry and Polymer Chemistry during her university studies at the Johannes Gutenberg Universität in Mainz, Germany and the University of Massachusetts in Amherst, USA. She moved into the field of Enzymatic Polymerizations during her doctoral research at the University of Bayreuth, Germany and the Universidade Federal do Rio Grande do Sul, Porto Alegre, Brasil. After a postdoctoral research stay at Polytechnic University in Brooklyn, NY, USA she started an independent research group at the University of Groningen.

Already early in her career Katja Loos was awarded two travel scholarships of the German Academic Exchange Service (DAAD) and she received the very prestigious Feodor Lynen Fellowship award of the Alexander von Humboldt Foundation to conduct her postdoctoral research. During her independent research career, on the basis of her unique approach in combining modern polymer synthesis, (macro) molecular self-assembly, and utilization of the arising structures the Netherlands Organisation for Scientific Research (NWO) has awarded her the prestigious VIDI grant in 2009 and VICI grant in 2014 and the German Research Council (DFG) the Eleonore Trefftz guest professorship within the scope of its excellency initiative.

Katja Loos is a Fellow of the Dutch Polymer Institute (DPI) and the Royal Society of Chemistry (RSC).